

# Surface storage dynamics in large rivers: Comparing three-dimensional particle transport, one-dimensional fractional derivative, and multirate transient storage models

Eric J. Anderson<sup>1</sup> and Mantha S. Phanikumar<sup>2</sup>

Received 8 November 2010; revised 17 July 2011; accepted 26 July 2011; published 13 September 2011.

[1] Large rivers are major conduits for sediment and nutrient transport and play an important role in global biogeochemical cycles. While smaller rivers received attention in recent decades for hyporheic exchange and nutrient uptake, fewer studies have focused on the dynamics of surface storage zones in large rivers. We investigate transport dynamics in the St. Clair River, an international river straddling the U.S.–Canadian border, using a combination of modeling and dye tracer studies. We describe a calibrated three-dimensional hydrodynamic model to generate (synthetic) breakthrough data to evaluate several classes of 1-D solute transport models for their ability to describe surface storage dynamics. Breakthrough data from the 3-D particle transport model exhibited multimodal behavior and complex dynamics that could not be described using a single first-order exchange coefficient—an approach often used to describe surface storage in transient storage models for small rivers. The 1-D models examined include multirate transient storage (MRTS) models in which storage zones were arranged either in series or parallel as well as 1-D models based on fractional derivatives. Results indicate that for 1-D models to describe data adequately, the timing of solute pulses that correspond to various in-channel features such as sandbars, islands or meander bends should be taken into account. As a result, the MRTS model with storage zones arranged in series (i.e., exchange rates triggered sequentially) provided the best description of the data. In contrast, fractional derivative models that assume storage zones were arranged in parallel failed to capture the multimodal nature of the breakthrough curves.

**Citation:** Anderson, E. J., and M. S. Phanikumar (2011), Surface storage dynamics in large rivers: Comparing three-dimensional particle transport, one-dimensional fractional derivative, and multirate transient storage models, *Water Resour. Res.*, 47, W09511, doi:10.1029/2010WR010228.

## 1. Introduction

[2] In recent years there has been an increased interest in solute transport processes in large rivers given their role in delivering nutrients, bacteria, and sediment to coastal regions (e.g., rivers in the US Midwest contributing to the Gulf of Mexico hypoxia) [Houser *et al.*, 2010; Smith and Tran, 2010; Tank *et al.*, 2008]. The emergence of water quality forecasting and management has made solute transport prediction a priority for the modeling community. Protection of public drinking water intakes, recreational beach closures, algal bloom, and invasive species investigations all require information on solute transport dynamics in rivers and the ability to make timely and accurate predictions at downstream receiving water bodies. There are several approaches for setting up a solute transport model, and the differences in modeling approaches can be significant, such

as in the development time and computational expense between a one-dimensional (1-D) advection-dispersion model and a fully three-dimensional (3-D) hydrodynamic Fickian/Lagrangian model. In addition, there are advantages and disadvantages associated with the chosen approach, relating to their ability to resolve key processes within the physical domain in relation to the particular interest of the investigation. Therefore, the choice of modeling approach can be integral to the success of the study, and an evaluation of different methodologies is necessary for an efficient and effective model. However, the setup and assessment of current solute transport models can be nontrivial, particularly when models of higher dimension and complexity are applied to large river systems.

[3] Significant progress has been made in describing solute transport in small to medium-sized rivers in the last few decades [Bencala and Walters, 1983; Briggs *et al.*, 2009; De Smedt *et al.*, 2005; Deng and Jung, 2009; Fernald *et al.*, 2006; Gooseff *et al.*, 2007; Marion and Zaramella, 2006; Phanikumar *et al.*, 2007; Salehin *et al.*, 2003; Schmid, 2003, 2004; Shen *et al.*, 2008; Worman, 2000]. A majority of these studies is based on the 1-D transient storage (TS) model [Bencala and Walters, 1983; Runkel, 1998; Runkel *et al.*, 1998] or its variants in which separate equations are

<sup>1</sup>Cooperative Institute for Limnology and Ecosystems Research, University of Michigan, Ann Arbor, Michigan, USA.

<sup>2</sup>Department of Civil and Environmental Engineering, Michigan State University, East Lansing, Michigan, USA.

solved for solute concentration in the main channel and the dead zones. Important parameters in the TS model include a first-order exchange rate of solute between the main channel and the dead zones ( $\varepsilon$ ,  $\text{s}^{-1}$ ), sizes (areas) of the main channel ( $A$ ,  $\text{m}^2$ ) and the dead zones ( $A_s$ ,  $\text{m}^2$ ), the dispersion coefficient ( $D$ ,  $\text{m}^2 \text{s}^{-1}$ ) and the average velocity of water in the reach ( $u$ ,  $\text{m}^2 \text{s}^{-1}$ ). Although some details of how TS model parameters may change with stream order or discharge are available in the literature [e.g., *D'Angelo et al.*, 1993], there is a dearth of tracer data and modeling for large rivers. In particular, efforts aimed at linking our understanding of small streams to large river systems are lacking. While there is no single, universally accepted criterion for classifying rivers into the small or large category, width-to-depth ratios ( $W/H$ ) and discharge ( $Q$ ) have been used in the past with the understanding that  $W/H > 50$  denotes large rivers [*Parsons et al.*, 2007]. As  $W/H$  ratios increase, fundamental shifts in the flow regime can be expected based on a balance of forces within the river channel that have important implications for mixing and transport of solutes; yet, results based on small stream experiments and modeling (e.g., nutrient uptake rates) are often extrapolated to large rivers as if there are no fundamental changes in the relative importance of various processes as width-to-depth ratios increase [*Tank et al.*, 2008]. From the point of channel morphology and sediment transport, *Church* [1992] classified small to intermediate channels as those in which individual bed particles greatly influence channel morphology (with features such as step pool and riffle pool sequences) while large channels are essentially hydraulically controlled and dominated by major bar development. The focus of many recent studies on small to intermediate rivers has been on describing solute transport in the presence of hyporheic exchange. As our understanding of hyporheic zone processes and groundwater-surface water interactions increased, conceptual models, based on more complex interactions between different types of storage zones (e.g., surface and hyporheic storage zones), have proved to be useful in describing solute transport and to quantify hyporheic exchange rates. For example, *Briggs et al.* [2009, 2010] applied a two-storage zone TS model to successfully separate the relative contributions of hyporheic and surface storage zones in a stream and to describe transport in a coastal stream network. In these models, the storage zones are assumed to be arranged in parallel leading to concurrent hyporheic and surface storage dynamics. Using mathematically similar sets of equations and the idea of flow elements/reactors arranged in series or in parallel, *Basagaoglu et al.* [2002] outline methods to describe tracer transport in heterogeneous porous media in the presence of complex flow networks. *Kadlec* [1994] used similar methods to describe lithium tracer transport in a free water surface wetland. Ideas involving multiple flow elements, zones or pathways, and multiple exchange rates have led to more general models for transport, including the multirate mass transfer (MRMT) models [*Haggerty and Gorelick*, 1995; *Haggerty et al.*, 2000], the continuous time random walk (CTRW) approach [*Berkowitz et al.*, 2002; *Berkowitz et al.*, 2006], and the fractional derivative models [*Benson*, 1998; *Wheatcraft and Meerschaert*, 2008]. An excellent review of these models with a focus on their equivalence is available by *Silva et al.* [2009]. Applications of CTRW models to solute transport in rivers are described by *Boano et al.* [2007]

and *Marion et al.* [2008], while fractional derivative models in the context of rivers are described in the literature [*Bradley et al.*, 2010; *Chakraborty et al.*, 2009; *Deng et al.*, 2006; *Ganti et al.*, 2010; *Shen and Phanikumar*, 2009; *Zhang et al.*, 2009].

[4] A major limiting factor in our ability to observe and model solute transport processes in large rivers is the high cost (material, manpower, and time) associated with tracer studies. While it is relatively easy to achieve cross-sectional uniformity of tracer concentration in small rivers (e.g., to justify the use of one-dimensional models), it would be prohibitively expensive to conduct a similar study on a large river (e.g., a river that is 0.5 km wide and 10 m deep). Recent applications, based on satellite observations [*Neal et al.*, 2009; *Smith and Pavelsky*, 2008] and advances in GPS and Doppler current profiling technology [*García et al.*, 2007; *Shen et al.*, 2010], have the potential to improve our understanding of large river processes. The complexity of in-channel features (islands, sand bars, meanders) and processes often calls for fully three-dimensional flow and transport models; however, 3-D models are not the most attractive choice from a management perspective since considerable investment in time and effort is needed to setup such models. Since one-dimensional models are relatively easy to setup and implement, a key question is whether any one of the several 1-D models, described above, has the ability to describe (1) the timing and (2) the average concentration in a large river accurately (the information often needed for management). Therefore, the aim of this paper is to evaluate several one-dimensional transport models using data generated from a calibrated, fully three-dimensional, hydrodynamic model of the St. Clair River. Our primary focus was on surface storage zones; however, observed tracer data from natural rivers includes contributions from both surface and hyporheic storage zones even if one type of storage is known to dominate overall transport. Since it is impossible to generate tracer data that include contributions from surface storage zones only using field-based approaches, a method is needed that allows us to address questions related to surface storage zones in large rivers. To resolve this issue of storage zone separation, we use a calibrated, three-dimensional flow and transport model to generate synthetic data that does not include any contributions from hyporheic storage. Our working assumption is that if the 3-D flow and transport models represent the observed physics reasonably well, then the synthetic data generated using the 3-D models also represent the essential features of surface storage zones.

[5] In order to evaluate 1-D multirate transient storage models, a 3-D hydrodynamic and particle transport model was calibrated to field observations of water levels, currents, and dye tracer measurements. The aim of these comparisons was to demonstrate that the 3-D models are able to describe the primary characteristics of mixing and transport in the river. The 3-D particle transport models were used to simulate two types of dye releases: Release A is an instantaneous surface "patch" release that attempts to simulate our 2009 field experiments. This simulation serves to test the 3-D particle transport model using field data. Release B is a hypothetical release in which particles were released over the width and depth of a cross section to facilitate comparisons with (and to evaluate) several 1-D transport models.

Using the synthetic data from release B, comparisons are made with 1-D MRTS and fractional derivative models.

**2. Methods**

[6] The St. Clair River is located in the Great Lakes and serves as the outflow for Lake Huron, straddling the international border between the U.S and Canada (Figure 1). The average discharge in the St. Clair River is  $\sim 5200 \text{ m}^3 \text{ s}^{-1}$ , wherein the water elevation drops 1 to 1.5 m over its 64 km length. River width varies from approximately 500 m to almost a kilometer with typical depths in the 7–10 m range ( $W/H > 50$ ). The unique geometry of the river makes it an ideal case to test 1-D and 3-D models, as it contains two

large islands and a series of channel bifurcations in a delta region, which empties into Lake St. Clair. Several models have been employed to estimate solute transport in the river. In this study, comparisons are made between different one-dimensional, fractional advection-dispersion models and a fully three-dimensional particle transport model to determine differences between the various modeling approaches and to establish which, if any, of the one-dimensional models are able to capture the observed physics in a large river system. The computational domain for all 3-D models includes the complete length of the river from the head at Lake Huron through the bifurcations of the delta region to Lake St. Clair. Since it is impractical to release tracer to achieve cross-sectional uniformity in tracer concentration

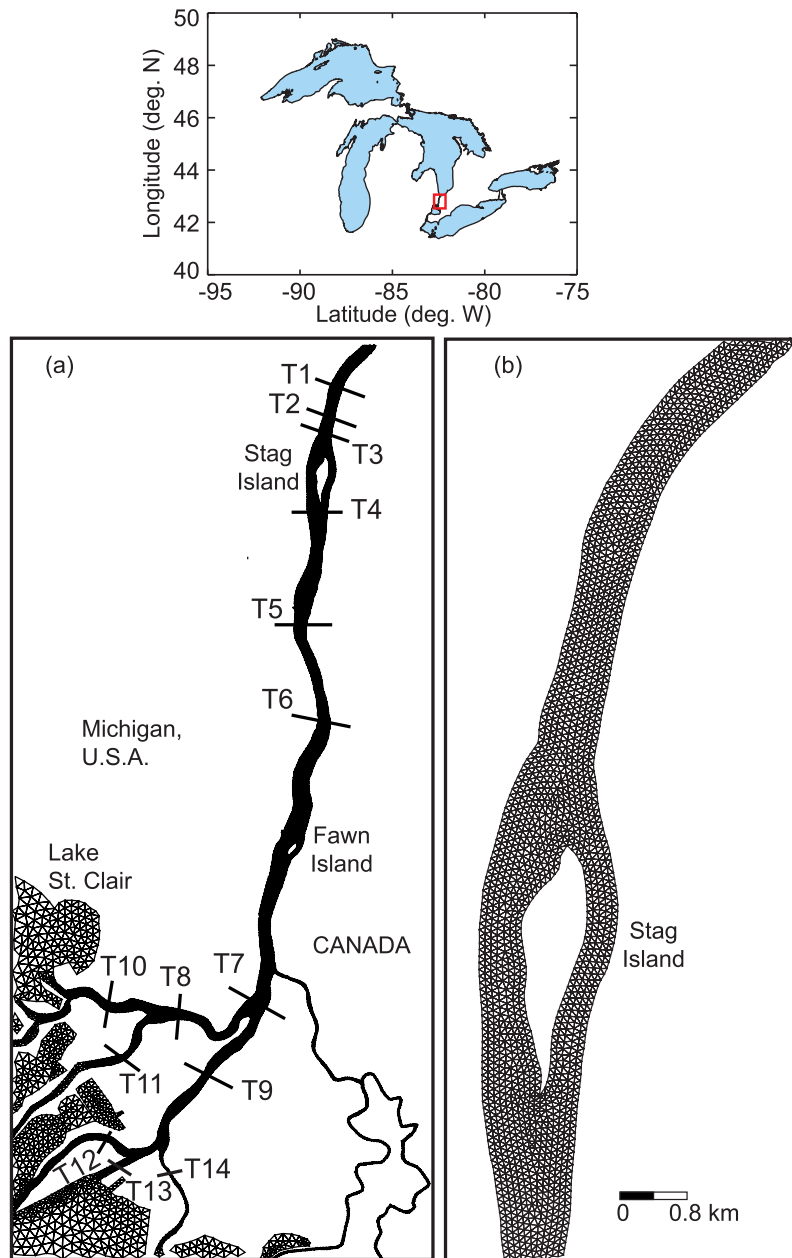


**Figure 1.** The St. Clair River located between Lake Huron and Lake Erie, with sampling transects for the observed and modeled solute transport scenarios.

(as is often done in small streams) at a release point that is on the order of 300 m wide with currents above  $1 \text{ m s}^{-1}$ , this approach was not attempted. Instead, a known amount of dye was released as a small patch in a predetermined region of the river, and comparisons were made between the observed and simulated dye plume shapes at downstream locations. The 3-D hydrodynamic model has been previously calibrated to observations of flows and currents in the river using a horizontal-looking acoustic Doppler current profiler (RD Instruments Workhorse 300 kHz H-ADCP) attached to the shore near the Blue Water bridge in Port Huron, Michigan (coordinates:  $42.9988^\circ\text{N}$ ,  $82.4252^\circ\text{W}$ ) [Anderson *et al.*, 2010]. In this work the calibrated model is compared to dye observations and used to generate breakthrough data for testing the 1-D models.

### 2.1. Dye Release

[7] A dye release was conducted on 18 August 2009. The release occurred near the center of the channel, in which 33.5 liters of a 21% concentration of Rhodamine WT were released at the surface over 20 s, yielding a measured initial concentration of approximately 105 ppb. Sampling was performed with three boats, each equipped with a submersible pump and in-series, flow-through fluorimeters (Turner Designs 10-AU field fluorometer). Near-surface samples (0.5 m below surface) were taken at eight downstream transects, which stretched across the entire width of the river. Fluorescence, temperature, absorbance, time, and location were recorded every 5 s as the boat traveled along each transect. In addition, vertical profiles of concentration were also recorded for three transects near the dye release location. During vertical sampling, the boat was allowed to drift with the plume, where efforts were made to make measurements near the location of the peak concentration within the plume. Drift tracks during this period were roughly 50 m long, and samples were taken from several points throughout the water column. Measurements of dye concentration were then compared to the 3-D, particle concentrations at these locations to gauge the amount of vertical mixing of the plume and the mixing length from the release point.

[8] Instrument calibration was performed in the lab with a series of solutions, correlating temperature and fluorescence readings with solution concentrations to provide corrected dye concentrations and to ensure no instrument drift. In addition, the effect of sunlight on the dye degradation was assessed by comparing two identical solutions, one sheltered from and the other exposed to sunlight. This test showed that a maximum of 12% degradation was possible on the day of the release, though it is expected that actual plume degradation would be less due to dispersion in the water column. Breakthrough curves of concentration (BTC) at each transect were generated from the dye observations for the surface layer at all transects and for the cross sections at the first three transects. Concentration, time, and location data were interpolated to a structured grid in order to spatially represent the plume in the 3-D model. The interpolated structured data was used to supply the concentration curves ( $C$  versus  $t$ ) for each transect and for comparison to the 3-D particle concentrations, described above. Velocity-corrected interpolations from time to the upstream datum were performed using a characteristic surface velocity from the transect location.

### 2.2. 3-D Particle Transport Model

[9] Hydrodynamics and three-dimensional solute transport in the river were modeled using the finite volume coastal ocean model (FVCOM) [Chen *et al.*, 2006] and a Lagrangian particle transport submodel. FVCOM is a three-dimensional, primitive equation, finite-volume model that solves the governing equations (equations (1) and (2)) and the Lagrangian particle transport equations (equation (3)) on unstructured grids:

$$\frac{\partial u}{\partial x} + \frac{\partial v}{\partial y} + \frac{\partial w}{\partial z} = 0, \quad (1)$$

$$\begin{aligned} \frac{\partial u}{\partial t} + u \frac{\partial u}{\partial x} + v \frac{\partial u}{\partial y} + w \frac{\partial u}{\partial z} - fv &= -\frac{1}{\rho_0} \frac{\partial P}{\partial x} + \frac{\partial}{\partial z} \left( K_m \frac{\partial u}{\partial z} \right) + F_u, \\ \frac{\partial v}{\partial t} + u \frac{\partial v}{\partial x} + v \frac{\partial v}{\partial y} + w \frac{\partial v}{\partial z} + fu &= -\frac{1}{\rho_0} \frac{\partial P}{\partial y} + \frac{\partial}{\partial z} \left( K_m \frac{\partial v}{\partial z} \right) + F_v, \\ \frac{\partial P}{\partial z} &= -\rho g, \end{aligned} \quad (2)$$

$$\begin{aligned} \frac{d\mathbf{x}}{dt} &= \mathbf{v}(\mathbf{x}(t), t), \\ \mathbf{x}(t) &= \mathbf{x}(t_n) + \int_{t_n}^t \mathbf{v}(\mathbf{x}(\tau), \tau) d\tau, \end{aligned} \quad (3)$$

where  $x$ ,  $y$ , and  $z$  are the Cartesian coordinates,  $u$ ,  $v$ , and  $w$  are the velocity components,  $\rho$  is density,  $\rho_0$  is a reference density,  $P$  is pressure,  $f$  is the Coriolis parameter,  $g$  is gravitational acceleration,  $K_m$  is the vertical eddy viscosity coefficient,  $F_u$  and  $F_v$  are the horizontal momentum diffusion terms, and  $\mathbf{x}(t) = x\mathbf{i} + y\mathbf{j} + z\mathbf{k}$ ,  $\mathbf{v}(t) = u\mathbf{i} + v\mathbf{j} + w\mathbf{k}$  are the particle position and three-dimensional velocity vectors at time  $t$ , respectively. The horizontal momentum diffusion terms in (2) have the form

$$\begin{aligned} F_u &= \frac{\partial}{\partial x} \left( 2A_m \frac{\partial u}{\partial x} \right) + \frac{\partial}{\partial y} \left( A_m \left( \frac{\partial u}{\partial y} + \frac{\partial v}{\partial x} \right) \right), \\ F_v &= \frac{\partial}{\partial y} \left( 2A_m \frac{\partial v}{\partial y} \right) + \frac{\partial}{\partial x} \left( A_m \left( \frac{\partial u}{\partial y} + \frac{\partial v}{\partial x} \right) \right), \end{aligned} \quad (4)$$

where  $A_m$  denotes the horizontal eddy diffusion coefficient. The governing equations (1) and (2) were solved in their sigma-coordinate form [Chen *et al.*, 2006]. The  $\sigma$  transformation maps the irregular bottom topography to the range  $-1$  (at the bottom) to  $0$  (at the top surface) thus providing a smooth representation. To close the primitive equations (1) and (2), horizontal and vertical mixing formulations are needed. The Smagorinsky formulation was used to compute the horizontal eddy diffusion coefficient  $A_m$  in (4) and the Mellor-Yamada turbulence closure scheme was used to estimate the vertical eddy viscosity  $K_m$  [Chen *et al.*, 2006]. The 3-D Lagrangian particle model was solved using a four-stage, fourth-order accurate explicit Runge-Kutta scheme, in which a random walk technique was used to account for subgrid-scale turbulent variability. A horizontal diffusion coefficient ( $D = 0.059 \text{ m}^2 \text{ s}^{-1}$ ) was applied for the St. Clair River, based on previous model calibrations [Anderson and Schwab, 2011; Anderson *et al.*, 2010]. The

3-D, hydrodynamic model of the St. Clair River used in this study was adapted from the Huron-Erie Connecting Waterways Forecasting System (HECWFS) [Anderson *et al.*, 2010], which is a real-time forecasting model for the St. Clair River, Lake St. Clair, and the Detroit River. For this investigation, horizontal resolution in the St. Clair was increased to 25 m to provide a finer-scale solution of particle transport throughout the river, with vertical resolution provided by seven evenly distributed sigma layers. Bathymetric data was taken from a 2000 NOAA survey at a horizontal resolution of  $\leq 100$  m and vertical accuracy of 0.5 m or 10% of the depth, whichever is smaller (as reported by *Holtschlag and Koschik* [2002]). Dynamic water levels from the head of the St. Clair River and mouth of the Detroit River were used to drive the flow through the model, in addition to an unsteady wind field and tributary inflows. Simulations were computed at a time step of 4 s, yielding a Courant Number  $\leq 0.1$ .

[10] Particle simulations for the 3-D hydrodynamic model were performed for two cases: (1) an instantaneous point release mimicking the dye tracer study (release A); and (2) an instantaneous “wall” of particles released in uniform concentration across the width and depth of the channel (release B). In release A, the hydrodynamic model was run for the period 18–19 August 2009, and particles ( $n = 100,000$ ) were instantaneously released at the surface in the center of the channel over a  $\sim 5$  m horizontal surface patch in order to match the initial conditions of the experimental dye release. Downstream particle concentrations were calculated for eight transects along the river using a cross-sectional weighted concentration in the top sigma layer,

$$\bar{C}(t) = \frac{\sum_{i=1}^N \forall_i C_i}{\sum_{i=1}^N \forall_i}, \quad (5)$$

where  $C_i$  is the particle concentration at time  $t$  in each cell,  $\forall_i$  is the volume of each grid cell, and  $N$  is the total number of cells across each transect. Results are compared to observations for concentration breakthrough curves at each transect, plume spread (lateral mixing) along the length of the river, and for vertical concentration profiles.

[11] In release B, simulations were performed for the same period and forcing conditions; however, the initial condition for particle locations was a uniform wall of particles that stretched across the river in uniform concentration. In this release, the particle wall was located at the same geographic location; however particles ( $n = 100,000$ ) extend across the entire width of the river and throughout the water column. This condition was applied to provide an even starting point for comparison to the 1-D models, in which spatially distributed releases cannot be resolved. Again, particle concentrations were calculated using equation (5), however the number of transects were extended into the delta channels as well to make comparisons between the 3-D and 1-D models in the presence of channel bifurcations. Transects in the main channel of the river, upstream of the bifurcations, are the same as those used in model validation from case (1). In addition to cross-sectional averages of

concentration, calculations were performed for surface concentrations (top layer) at a specific cross-channel location (i.e., a specific “point” in the river). With this addition, we determined how much the concentration at a specific location deviates from the cross-sectional average, and further evaluated the differences between 1-D and 3-D estimates of solute transport.

## 2.3. One-Dimensional Solute Transport Models

### 2.3.1. Space-Fractional ADE/TS Models

[12] As a starting point for introducing the different 1-D models, consider the following TS model in which the second-order dispersion term is replaced with space-fractional dispersion terms. Since power law jumps of particles in space are governed by space-fractional derivative models and power law jumps in time lead to fractional-in-time models, the motivation for using space-fractional derivatives was to capture the early breakthrough (relative to Fickian dispersion) of tracer data:

$$\begin{aligned} \frac{\partial C}{\partial t} + u \frac{\partial C}{\partial x} &= D \left[ q \frac{\partial^\alpha C}{\partial x^\alpha} + (1-q) \frac{\partial^\alpha C}{\partial (-x)^\alpha} \right] \\ &\quad + \frac{q_L}{A} (C_L - C) + \varepsilon (C_S - C), \quad (6) \\ \frac{\partial C_S}{\partial t} &= \varepsilon \frac{A}{A_S} (C - C_S). \end{aligned}$$

Here  $1 \leq \alpha \leq 2$  is the fractional exponent and  $0 \leq q \leq 1$  is a parameter that controls the bias of the dispersion term (forward for  $q = 1$  versus backward dispersion for  $q = 0$ ). Equation (6) reduces to the fractional advection-dispersion equation (FADE) for  $\varepsilon = q_L = 0$  and the well-known TS model [Runkel, 1998] for  $\alpha = 2$  and  $q = 1$ . The well-known TS model in (6) is based on a single-rate mass transfer model with an exponential residence time distribution (RTD) of solute particles in the storage zones, which may not adequately describe the deeper hyporheic flow paths, known to follow a power law RTD [Gooseff *et al.*, 2005]. To describe solute transport in the presence of significant hyporheic exchange, Gooseff *et al.* [2005, 2007] modify equation (6) by including the convolution of a user-specified RTD (the hyporheic memory function) with the solute concentration in (6). It is known that the shape of tracer BTCs in large rivers is not controlled by hyporheic exchange and sediment properties [Deng *et al.*, 2010]. For the St. Clair River, estimates of groundwater discharge into the channel [Gillespie and Dumouchelle, 1989] were found to be small ( $\sim 0.3 \text{ m}^3 \text{ s}^{-1}$  by area). As the data used for testing the 1-D models were generated using 3-D particle transport models for the channel, hyporheic exchange was not considered in this work.

[13] Several researchers used the FADE to fit tracer data from natural streams [Chakraborty *et al.*, 2009; Deng *et al.*, 2004] using maximally negative skewness ( $q = 0$ ). While the meaning of dispersion in the negative coordinate direction (i.e., opposite to the flow direction) is open to interpretation, Baeumer *et al.* [2009] and Chakraborty *et al.* [2009] discuss space-time duality associated with fractional derivative models and note that from a particle perspective, falling behind is mathematically equivalent to getting trapped (as in a river dead zone). Shen and Phanikumar [2009] used (6)

with  $q = 1$  (forward dispersion) to describe the early breakthrough of tracer data in Grand River, Michigan, and used a single, scale-invariant, dispersion coefficient (instead of using different  $D$  values in the reaches) over a 30 km length of the river. We use the FSTS model with maximally negative skewness ( $q = 0$ ) to describe the St. Clair River data as described below. Application of the FADE with  $q = 0$  is discussed by *Chakraborty et al.* [2009]. The motivation for modifying the FADE to include a storage zone as in equation (6) was that the storage term with a single rate may capture shallow surface storage while the fractional dispersion term with maximally negative skewness may capture “deeper” surface storage that cannot be described using a single rate.

[14] The fractional-in-time ADE (FADE) [*Schumer et al.*, 2003] can be used to describe the total solute concentration in the river following a fractional order mobile-immobile model (MIM):

$$\frac{\partial C}{\partial t} + \beta \frac{\partial^\gamma C}{\partial t^\gamma} + u \frac{\partial C}{\partial x} = D \frac{\partial^2 C}{\partial x^2}, \quad (7)$$

where  $\beta$  is the capacity function,  $\gamma$  is the fractional time derivative order, and  $u$  and  $D$  are the velocity and dispersion coefficients for the river (i.e., solute in the mobile phase). Equation (7) can be used to describe power law BTCs in streams for the total concentration, and results from two separate fractional-derivative equations for the mobile ( $C_m$ ) and immobile ( $C_{im}$ ) zones as described by *Schumer et al.* [2003]:

$$\begin{aligned} \frac{\partial C_m}{\partial t} + \beta \frac{\partial^\gamma C_m}{\partial t^\gamma} + u \frac{\partial C_m}{\partial x} &= D \frac{\partial^2 C_m}{\partial x^2} - \beta C_{m0} \frac{t^{-\gamma}}{\Gamma(1-\gamma)}, \\ \frac{\partial C_{im}}{\partial t} + \beta \frac{\partial^\gamma C_{im}}{\partial t^\gamma} &= \beta C_{m0} \frac{t^{-\gamma}}{\Gamma(1-\gamma)}, \end{aligned} \quad (8)$$

where  $C_{m,0}(x, t = 0) = C_{m,0}(x)$ ,  $C_{im,0} = 0$  and  $f(t) = t^{-\gamma}/\Gamma(1-\gamma)$  is the power law memory function. See *Schumer et al.* [2003] and *Zhang et al.* [2009] for more details about this model.

[15] Finally, we consider two multirate mass transfer models (called herein multirate transient storage models or MRTS), which are generalizations of (6). One model assumed storage zones arranged in parallel (i.e., concurrent) while the second model assumed storage zones triggered at different times  $t_j^*$  (i.e., sequentially or arranged in series).

### 2.3.2. MRTS Model With Storage Zones in Parallel

[16] For the MRTS model with parallel storage zones, solute concentration is described as

$$\begin{aligned} \beta_0 \frac{\partial C_m}{\partial t} + \sum_{j=1}^N \beta_j \frac{\partial C_{im,j}}{\partial t} &= D \frac{\partial^2 C_m}{\partial x^2} - u \frac{\partial C_m}{\partial x} = \mathcal{L}(C_m), \\ \frac{\partial C_{im,j}}{\partial t} &= \alpha_j (C_m - C_{im,j}) \quad j = 1 \dots N. \end{aligned} \quad (9)$$

The parameters  $\beta_j$  are the capacity coefficients to account for the mass in the storage zones (immobile regions) while  $\beta_0$  is the capacity coefficient for the river. In TS terminology,

$\beta_0$  is the cross-sectional area of the stream channel ( $A$ ),  $\beta_j$  are the sizes (areas) of the storage zones and

$$\alpha_j = \left( \frac{A}{A_{S,j}} \right) \varepsilon_j \quad (10)$$

are the first-order exchange coefficients associated with the  $j$ th storage zone. There is no confusion between the  $\alpha_j$  in the above equation and the fractional derivative exponent ( $\partial^\alpha$ ) in equation (6). Equation (9) reduces to the TS model in (6) for one storage zone.

### 2.3.3. MRTS Model With Storage Zones in Series

$$\beta_0 \frac{\partial C_m}{\partial t} + \sum_{j=1}^N \left[ \mathcal{H}(t - t_j^*) - \mathcal{H}(t - t_{j+1}^*) \right] \beta_j \frac{\partial C_{im,j}}{\partial t} = \mathcal{L}(C_m),$$

$$\frac{\partial C_{im,j}}{\partial t} = \alpha_j (C_m - C_{im,j}) \quad j = 1 \dots N. \quad (11)$$

[17] In (11),  $\mathcal{H}(\cdot)$  denotes the Heaviside step function and all other symbols are explained above. Equations (9) and (11) were solved using a fourth-order accurate compact scheme with spectral-like resolution [*Phanikumar et al.*, 2007]. Since the Heaviside step function has the property

$$[\mathcal{H}(x - a) - \mathcal{H}(x - b)]f(x) = \begin{cases} 0 & \text{if } x < a \\ f(x) & \text{if } a \leq x \leq b, \\ 0 & \text{if } x > b \end{cases} \quad (12)$$

at any given time, the summation term over all immobile zones reduces to the contribution from a single ( $j$ th) immobile zone for  $(t_j^* \leq t \leq t_{j+1}^*)$ . The model in equations (11) has additional timing parameters ( $t_j^*$ ), which are absent in model (9). The space-fractional derivatives in equation (6) were approximated using the Caputo derivative and a finite-volume approximation as described by *Shen and Phanikumar* [2009].

## 3. Results

### 3.1. Dye Observations and 3-D Particle Transport Model Verification

[18] A comparison of the observed and simulated flows and surface currents in the river (Figure 2) [*Anderson et al.*, 2010] shows that the hydrodynamic model was able to describe the key features reasonably well. Modeled currents from the top two surface layers were used in the comparison with the ADCP data from similar depths. Additional comparisons with observed data are available [*Anderson et al.*, 2010]. These comparisons essentially indicate that the model does a reasonable job of describing the observed flows and water surface elevations, while currents are somewhat underpredicted. Several factors could have contributed to this difference including (1) uncertainty in the bathymetry [*Holtschlag and Koschik*, 2002], (2) limitations of horizontal and vertical resolution or turbulence schemes employed in resolving turbulent flow fields in the river, and (3) uncertainty involved in the ADCP observations. However, based

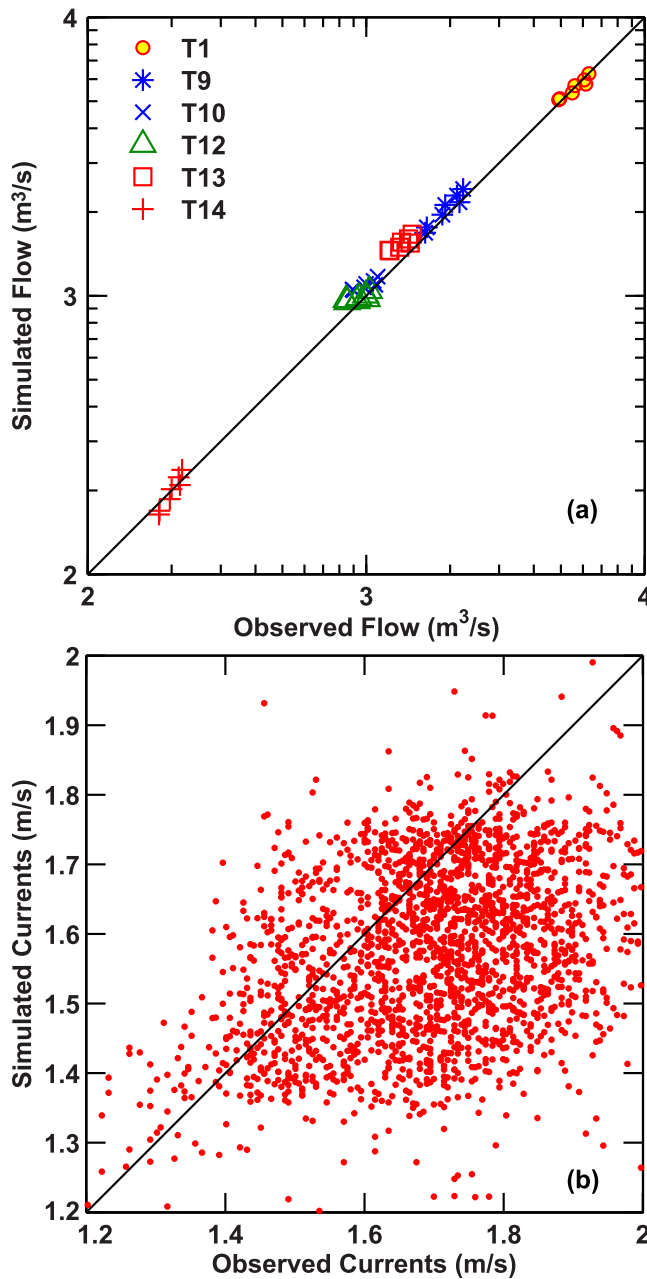


**Figure 2.** Results based on the 3-D hydrodynamic model: (a) comparisons between observed (H-ADCP) and simulated flows (notice the log-log scale) and (b) surface currents in the St. Clair River.

on the detailed comparisons and flow statistics for the hydrodynamic model presented by *Anderson et al.* [2010], our overall assessment is that the model can be used for further analysis of flow and transport in the St. Clair River.

[19] For a surface (center channel) dye release in the St. Clair River on 18 August 2009, the travel time of the plume from the release point to the last measured transect (just upstream of the delta bifurcations) was 10.5 h. Comparisons of weighted-average tracer breakthrough from the 3-D particle transport model (with initial conditions and plume reconstruction obtained by sampling the plume as shown in Figures 3a and 3b and the observations at each transect

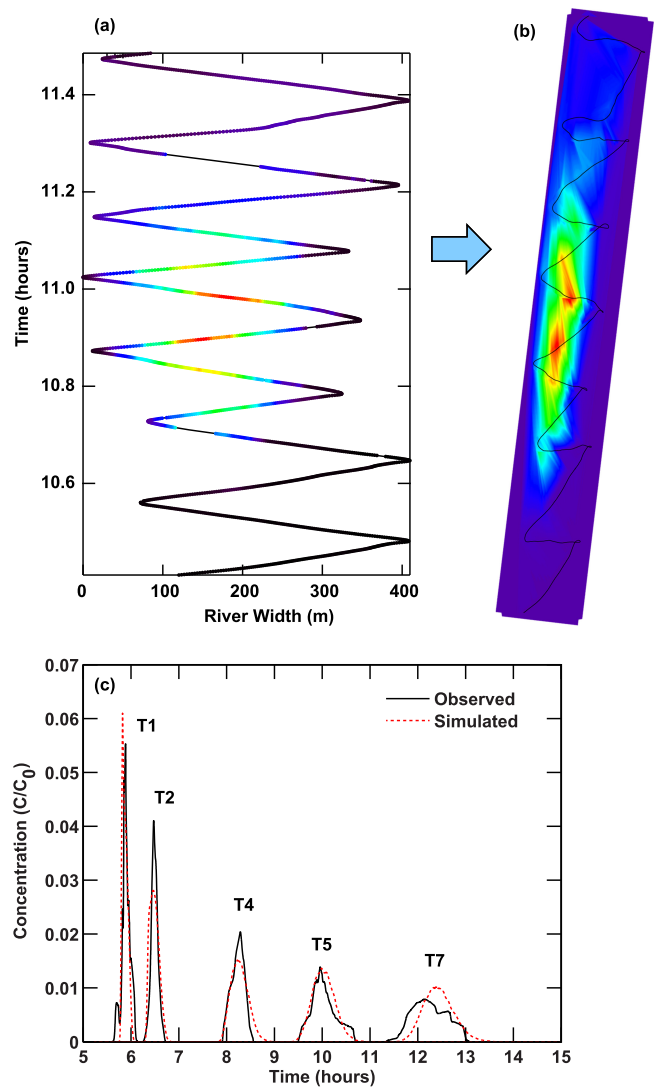


**Figure 3.** Comparison between observed Rhodamine WT concentrations and simulations based on the 3-D particle transport model. (a) Details of plume sampling showing the boat tracks. (b) Interpolated plume shape. (c) Weighted cross-sectional averages of concentration at each observation transect are shown (observed—solid line in black; model—dashed line in red). Concentrations are normalized to the initial concentration at the release point.

show a reasonable agreement in plume dispersion and timing (Figure 3c). Our tracer observations probably include contributions from fast hyporheic flow paths as well; however, since our particle tracking simulations do not include any flow paths outside the channel (due to the kinematic condition of zero normal velocity at the bottom and the sides), the comparison in Figure 3c serves to bring out the effects of hyporheic exchange on solute BTCs over the time scales relevant to this study. Longitudinal dispersion of the plume causes the exposure time to increase from 20 min at the first transect to over 2 h at the last measured transect. The predicted leading edge of the plume is in nearly perfect agreement with the observations for all transects except the last transect, in which a 15 min lag develops. Peak concentration for each transect, based on weighted

cross-sectional averages, is in reasonable agreement for the observed and predicted values. Both resolve the rate of decay, though the model appears to underpredict the peak concentrations for two upstream transects, and overpredict the concentration at the last transect.

[20] Lateral mixing in the river is also represented for the observed and predicted plumes (Figure 4). The western edge and maximum concentration pathways are in agreement for the observed and modeled releases with little variance in lateral spread across the river aside from a noticeable reflection at the western boundary near 5 km downstream of the release point. The eastern edge of the plume, which is at much lower concentrations, does begin to extend across the river at this point.

[21] Vertical mixing of the plume occurs much faster relative to lateral dispersion, as the dye reached a well-mixed condition in the water column by the second transect (Figure 5). Observations at three transects show the dye to vertically mix between transects 1 and 2 (between 2 and 4 km downstream of the release), while at transect 1 the plume is still highly concentrated near the surface. The modeled particle release predicts mixing to occur slightly faster than the observed plume; at transect 1 the plume has begun to mix into the water column, giving a near-linear distribution. However, even in the modeled release, total vertical mixing does not occur until between 3 and 4 km downstream of the release. These comparisons indicate that the 3-D hydrodynamic and particle transport models are able to reproduce the principal mixing characteristics of the dye plume observed during the tracer study; however, it is clear that the 3-D models simulate processes that are very different from what typical 1-D models incorporate. Several factors could have contributed to the differences in the shapes of observed and simulated BTCs in Figure 3c including uncertainty in bathymetry, uncertainties in the tracer mass and the initial shape of the dye patch during the release (i.e., initial conditions; see Figures 3a and 3b), and limitations of

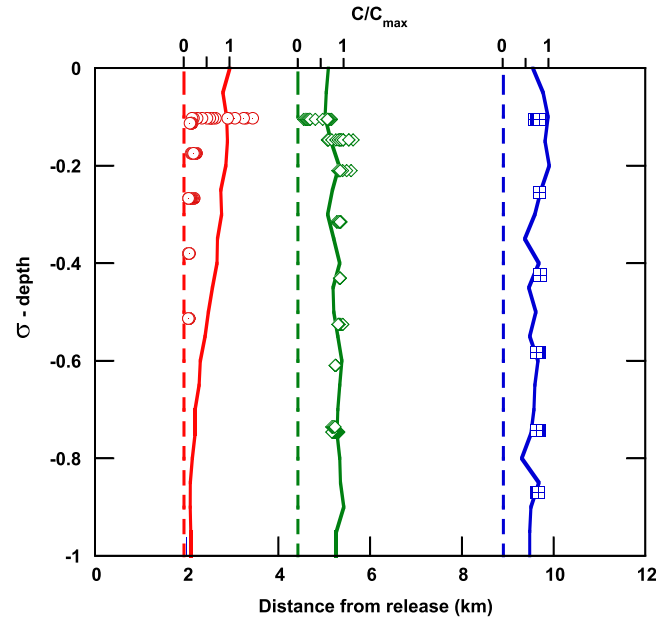


**Figure 5.** Vertical profiles of concentration for the observed dye release (symbols) and 3-D model predicted particle concentrations (solid lines). Profiles are shown as a function of sigma depth and distance (1.94, 4.43, and 8.90 km, respectively) from the release point. Concentrations are scaled with the maximum concentration in each vertical transect extending from the surface to the bottom.

turbulence schemes used to parameterize horizontal and vertical mixing coefficients. The mismatch (between model and reality) in the descriptions of initial plume shape and size, tracer mass, and turbulence processes is likely responsible for overpredicting/underpredicting concentrations in the 3-D models. A detailed evaluation of the turbulence models is not the focus of this work and additional details

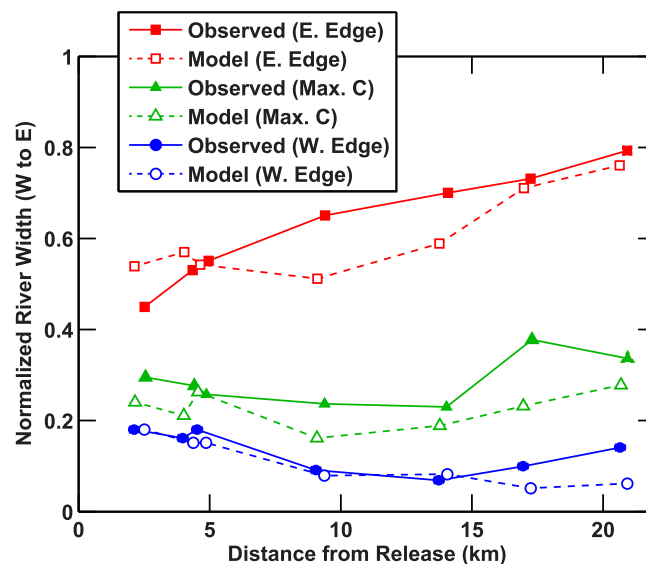


**Figure 4.** Lateral spreading of the plume as it drifts downstream. Values for each transect are plotted for normalized distance from western (0) to eastern (1) shore for the plume western edge, eastern edge, and point of maximum concentration for the dye observations and modeled particle plume.



can be found by *Pope* [2000]. Despite the complexities involved, the comparisons in Figures 3 and 4 serve to demonstrate that the 3-D models capture the general features of transport. Therefore, in order to evaluate the various 1-D models focusing on surface storage dynamics, we use the synthetic data generated from the calibrated 3-D models as described above.

### 3.2. Comparison of 3-D Particle Transport and 1-D Solute Transport Model Simulations

[22] Once the 3-D hydrodynamic and particle transport models are tested based on field data, the models can be used with some confidence to generate breakthrough data for scenarios that are difficult to realize in a field setting. For example, we simulated the release of particles across the depth and breadth of the river to create well-mixed conditions by minimizing the length of the mixing zone and to facilitate the application of 1-D models. Therefore, the data generated is a result of surface storage dynamics alone and shows (Figure 6) several interesting features including bimodal/multimodal breakthrough curves which cannot be adequately described using the standard TS model with a single exchange rate. Surface storage in small streams is known to follow exponential RTD [*Gooseff et al.*, 2005] ( $C \sim e^{-at}$ ); a plot of  $\ln(C)$  versus time can be used to determine the exponent  $a$ . For a power law residence time distribution (RTD) ( $C \sim t^{-k}$ ), a plot of  $\log_{10}(C)$  versus  $\log_{10}(t)$

can be used to estimate  $k$ . Figure 6b shows log-log plots of the normalized, cross-sectional average concentration versus time; the BTCs exhibit different slopes for intermediate and late times. Power law fits with slope  $k \sim 3$  for intermediate times and  $k \sim 16$  for late times describe the data better than exponential fits (not shown); however, a single rate could not be used to describe the data. An important aspect of the BTCs is their multimodal nature. While the power law or lognormal fits can be used to describe the slopes for intermediate and late times in an average sense, none of the fits take the multimodal nature of the BTCs into account which was probably an indication that a fundamental feature of solute transport in the river was not taken into account. Since a great deal is already known about the late-time behavior of BTCs and the appropriate models [*Haggerty et al.*, 2000], our primary focus was on intermediate times and in understanding which, if any, of the 1-D models can capture the multimodal BTCs; therefore comparisons are shown in linear as opposed to log scale (to emphasize the peaks and the multimodal behavior).

[23] Before proceeding with detailed comparisons, we examine snapshots of tracer plumes (cross-sectional average concentration) in the river to understand the physical processes responsible for the multimodal BTCs. Figures 7a–7f show the evolution of tracer plumes generated from the 3-D particle transport model around Stag Island at increasing travel times with Figure 7a corresponding to the

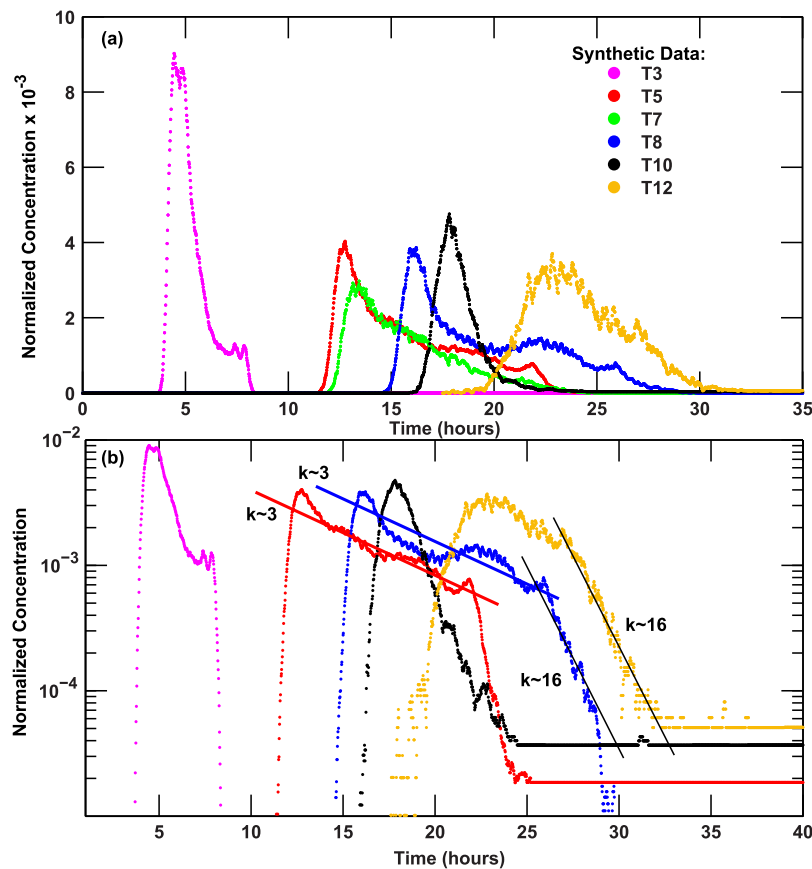


**Figure 6.** Tracer breakthrough data generated using the 3-D particle transport model for testing the one-dimensional models: (a) linear scale and (b) log-scale. Weighted cross-sectional average concentrations normalized to their initial values are plotted.

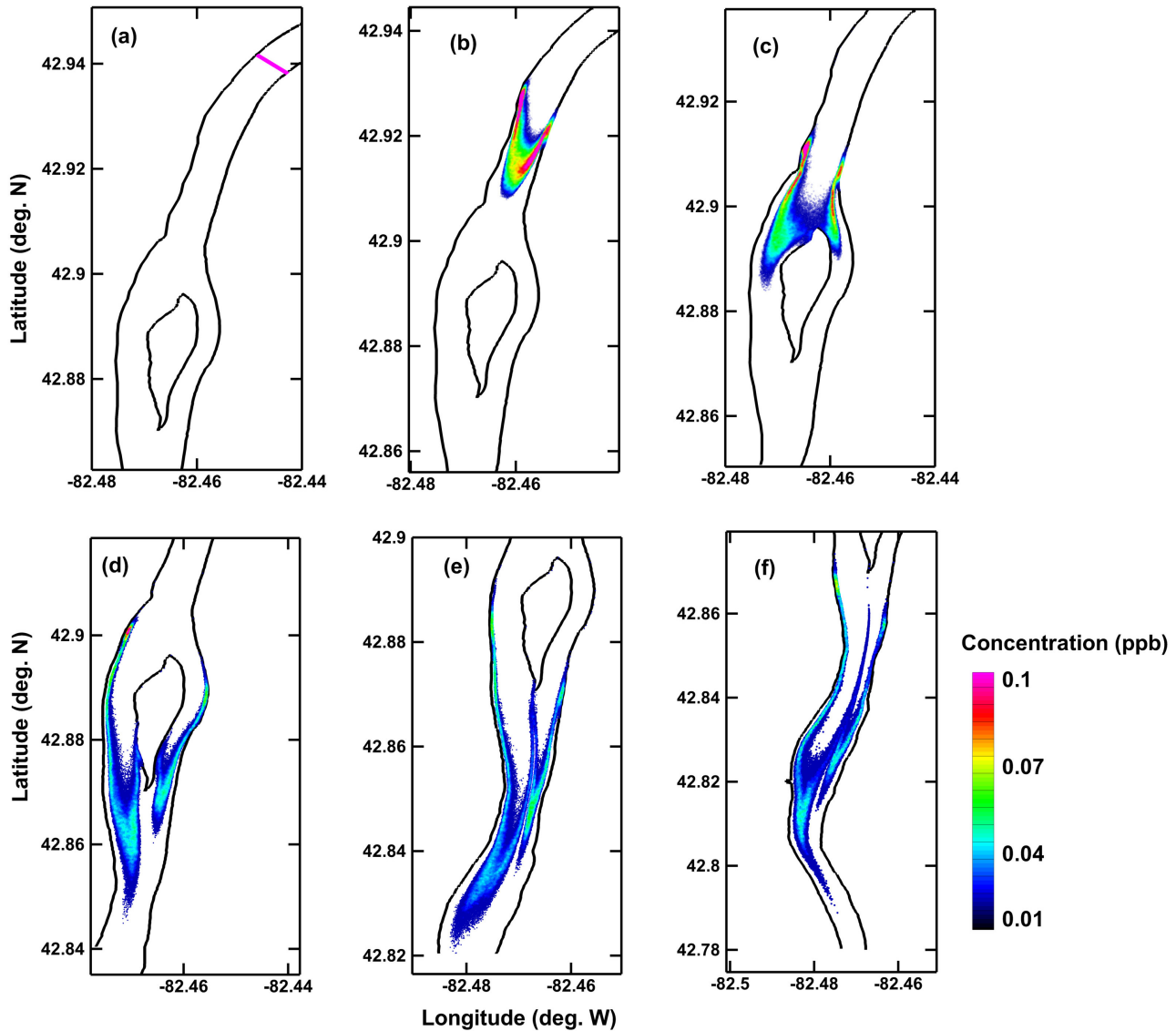


**Figure 7.** Spatiotemporal evolution of the dye cloud as it travels past Stag Island in the St. Clair River. Notice how river features including the island and a meander bend produce a mixing pattern in which relatively high concentration regions of the plume lag behind areas with lower concentration producing multimodal breakthrough curves at downstream sampling locations.

initial time of release ( $t = 0$ ). It is clear that the orientation of the channel and the flow field are such that even at early times following tracer release (Figures 7b and 7c) regions of relatively high concentration (red) lag behind low concentration regions (blue). These high concentration regions of the plume later appear as peaks in the BTCs. River features such as islands and meander bends are also responsible for the observed shape of the BTCs. For example, as the flow bifurcates before the island in Figure 7c and the two branches merge further downstream, the velocity distribution in the two branches are such that regions of relatively high tracer concentration lag behind low concentration regions (e.g., in Figure 7e notice that the dark blue region of the plume is in front of the cyan-colored region of relatively high concentration coming out of the right side branch). We therefore conclude that such multimodal BTCs are an essential aspect of river systems characterized by complex

features including islands and meander bends. In what follows, we seek to identify 1-D model(s) that can capture this aspect of the observed BTCs. Breakthrough curves generated at diagnostic nodes in the top layer resembled the cross-sectional average BTC presented in Figure 6 although the concentration values were higher; therefore the data is not presented.

[24] Figure 8 shows the different 1-D MRTS model solutions plotted on top of each other for station T8 (Figure 1). The station was selected as the breakthrough data clearly show a multimodal behavior. We evaluated different MRTS models with the number of storage zones increasing from one to five. The 5-zone “parallel” model (in which all storage zones trap and release solutes concurrently but at different exchange rates) describes the data in an average sense ( $RMSE = 7.6 \times 10^{-5}$ ) but fails to describe any of the individual peaks. This result may be acceptable for some

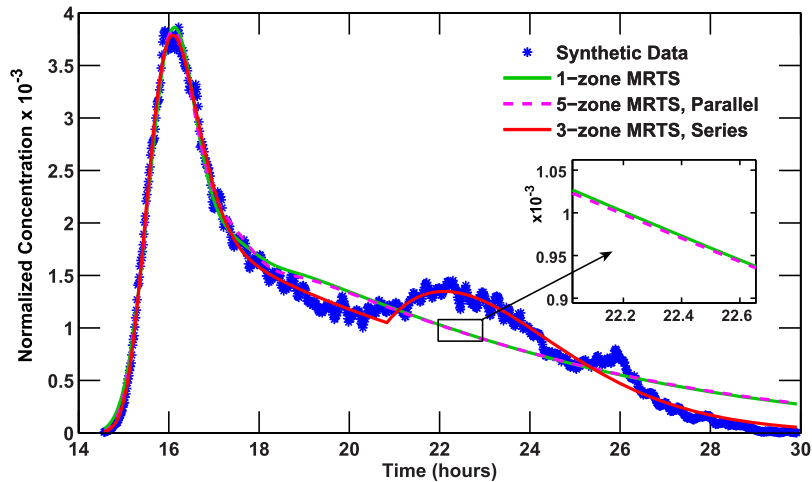


**Figure 8.** Comparison of 1-D MRTS solute transport models with synthetic data generated from a 3-D particle transport model. Note that for the parallel MRTS model there is no improvement in solution by adding more storage zones beyond the first zone. Information about how storage zones are connected (e.g., series versus parallel) is key to improving solute transport predictions.

types of solutes but not all (e.g., peaks may be important while modeling bacteria, viruses, and toxic substances). The 3-zone series MRTS model describes the data better (compared to the 5-zone parallel MRTS model) and captures the multimodal behavior as well ( $\text{RMSE} = 2.9 \times 10^{-5}$ ). Further examination of the solutions indicated that the timing of different pulses is important to accurately model solute transport in this large river. This information is included in the series version of the MRTS model using the Heaviside step functions. Figure 8 shows that there is no improvement in the parallel MRTS model solutions from a single zone model and a 5-zone model (they are identical in the inset close-up view) which shows that the model fails to converge to the data as the number of storage zones is increased; however, a 3-zone series model was found to describe the data well. This indicates that the

parallel-zone MRTS model fails to capture a fundamental aspect of the transport processes—the arrangement of the storage zones. If this key detail is incorporated into the model, then the data can be described using relatively few (as few as two or three) storage zones. Results based on the five zone parallel MRTS model and the fractional derivative FSTS model are plotted in Figure 9. The models produced identical solutions at late time. The fractional-in-time ADE (FSADE) model produced qualitatively similar results. This is not surprising since both (FSTS and FSADE) models conceptualize the storage zones as being arranged in parallel. A closer examination, however, showed that the FSADE model with  $0 \leq \gamma \leq 1$  is not suitable for describing the BTCs since the slopes at intermediate and late times at station T8 were steeper than  $t^{-2}$  [Schumer *et al.*, 2003]. Therefore the FSADE solutions are not

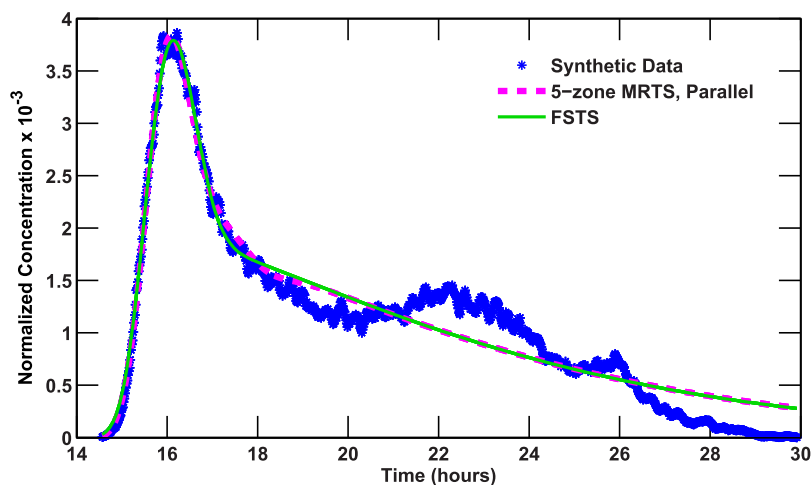


**Figure 9.** Comparison of 1-D solute transport models FSTS and 5-zone parallel MRTS models with synthetic data generated from a 3-D particle transport model. The late time behavior of the transient storage model based on space fractional dispersion (FSTS model) with maximally negative skewness ( $q = 0$ ) is identical to the multirate model; neither model captured the multimodal nature of the BTC.

presented. Since the series MRTS model has additional parameters corresponding to the “trigger times” ( $t_j^*$ ), a key question is if the inclusion of these additional timing parameters is justified relative to the improvement in the solution. To answer this question, and to address the more general question of comparing the performance of models with different parameters, the Akaike information criterion (AIC) was computed for all model runs, results are tabulated in Table 1. The AIC [Burnham and Anderson, 1998], which is based on the principle of parsimony and information theory, penalizes models with a large number of parameters; therefore, the model is selected with the lowest AIC value. We used the following definition of AIC:

$$AIC = n \ln \left( \frac{SSE}{n} \right) + 2K, \tag{13}$$

where  $n$  = the number of data points,  $SSE$  = sum squared error between the model and the observed data, and  $K$  = the number of estimated parameters ( $P$ ) plus a model variance parameter ( $K = P + 1$ ). The model with the smallest AIC value represents the best choice among all models considered (if the AIC is negative, the model with the largest AIC after removing the negative sign represents the best choice). Clearly, use of the series MRTS model with three storage zones is justified considering the gain in the quality of the solutions from a single storage zone model. From Table 1 we notice that the series MRTS model with three zones represents the best model for station 8 (lowest AIC). There was a significant improvement in model performance as the number of storage zones increased from one to three but the gains became incremental as more zones were added. We considered a five zone series MRTS model as well. The model was able to describe the third peak in the BTC around 26 h in Figure 8. However, results for this case were not shown as the gains were found to be incremental. According to the AIC criterion, the improvement in model performance from three to five zones is offset by the additional parameters added to the model. Similar results were obtained for other stations as well. The insights gained from this work may be useful in constructing transport

models for large rivers based on new approaches (e.g., non-local theories). The series MRTS model suffers from the same drawback as the standard TS model that is widely in use—the model parameters change with river discharge. It may be possible to construct parsimonious continuous time random walk (CTRW) or fractional derivative models that capture the key aspects of the series MRTS model (e.g., using different transition time distributions  $\psi(t)$  in a CTRW model).

**4. Discussion**

[25] Comparisons between the 3-D particle transport model and field observations for the instantaneous surface “patch” release (release A) mimicking the 2009 field experiments indicate that the model was able to capture the principal characteristics of transport in the river (Figures 3, 4, and 5); the comparisons also serve to demonstrate the complexities involved in 3-D solute transport modeling. Model results for release B (in which a wall of particles was released to create well-mixed conditions) showed multimodal BTCs (Figure 6); however, tracer observations in Figure 3 showed only weakly bimodal BTCs (e.g., transect T7), and this feature was absent in the modeled BTCs for release A. Several factors could have contributed to this difference. Since releases A and B are fundamentally different, it is possible that the differences in the initial conditions (and hence the lengths of mixing zones and concentration histories) were responsible for the different BTCs in the two cases. The absence of a weakly bimodal feature (observed for station T7) in the simulated BTC in Figure 3 is probably related to a combination of factors including errors in sampling the dye plume shape and size (initial condition for the 3-D model) and inadequacies in the turbulence models employed (which influence transport through the parameters  $A_m, K_m$ ). Figures 3a and 3b clearly show the tradeoffs involved in sampling the dye plume in a fast-flowing river—while closely spaced transects improve the accuracy of the interpolated plume, the approach can be time consuming which is a major disadvantage since it is possible to completely miss the plume by the time the

**Table 1.** Summary of 1D Model Parameters Estimated for Stations T5 and T8

Station	Model	$u^a$ (m s <sup>-1</sup> )	$D$ (m <sup>2</sup> s <sup>-1</sup> )	$\alpha$	$q$	$A_{S_j}(j = 1 \dots N)$ (m <sup>2</sup> )	$\varepsilon_j(j = 1 \dots N)$ $\times 10^{-7}$ (s <sup>-1</sup> )	$t_j^*$ (s)	RMSE	AIC
T5	FSTS	0.73	0.69	1.32	0	1863.79	311.72	–	5.09E-05	–14,992.25
T8	FSTS	0.79	13.18	1.99	0	1940.49	281.35	–	7.67E-05	–17,458.65
T5	TS (1-zone)	0.80	17.27	2	–	1803.37	390.082	–	5.66E-05	–14,833.00
T8	TS (1-zone)	0.77	16.96	2	–	2008.77	286.33	–	7.67E-05	–17,461.00
T8	MRTS series (3-zone)	0.81	8.16	2	–	365.80 11,069.50 9352.20	883.65 1098.70 8099.84	54,741.82 75,005.71	2.93E-05	–19,222.00
T8	MRTS parallel (5-zone)	0.88	3.97	2	–	0.11 726.30 100.70 2046.70 113.40	7.01 6160.09 9123.86 327.80 9887.67	–	7.60E-05	–17,461.00
T5	MRTS parallel (5-zone)	0.98	1.46	2	–	1949.40 391.80 255.50 336.10 227.10	439.65 9992.60 6846.16 8934.70 588.99	–	5.31E-05	–15,004.00

<sup>a</sup>Discharge  $Q = 5000 \text{ m}^3 \text{ s}^{-1}$ .

survey is completed. Our objective in comparing the 3-D particle transport model with real data was to ensure that the model can describe the general features of transport observed in the river despite uncertainties in model inputs.

[26] Comparison of several 1-D solute transport models with BTCs generated using a 3-D particle transport model in the St. Clair River indicated that details of how the storage zones are conceptualized is important for the success of the modeling. We found that the standard TS model based on a single exchange rate was inadequate for describing the complex surface storage dynamics in the river. MRTS models, which are generalizations of the standard TS model, were found to describe the data better; however the storage zones should be conceptualized as arranged in series rather than in parallel. The series version of the MRTS model takes a fundamental aspect of large river solute transport; since transport is hydraulically controlled, at any given time, the BTC is controlled by one (or conceivably a few) dominant river feature(s) or storage zone(s). In other words, all storage zones in the river segments upstream of the plume do not exert the same level of influence on the BTCs at downstream locations; therefore it is not surprising that the parallel MRTS model fails to converge to the data as more storage zones are added. The space- and time-fractional derivative models considered in this paper conceptualize the storage zones as arranged in parallel; hence they do not describe the multimodal nature of the BTCs. There are significant differences in the solutions from space- and time-fractional derivative models as described by *Zhang et al.* [2009]. For example, the space-fractional dispersion term in the FSTS model (equation (6)) is used to describe retention here, but the model has no ability to distinguish between solutes in the mobile and immobile zones (solute remains in the mobile phase for all time). The time-fractional ADE model (equation (7)) can distinguish between solute in the two zones; however, the analytical solution for (7) at late time has a slope of  $t^{-1-\gamma}$  [*Schumer et al.*, 2003] and slopes for both intermediate and late times in the St. Clair River were found to be steeper than  $t^{-2}$ . The FSTS model was found to describe the data in an average sense although individual peaks could not be captured. The AIC for the FSTS model is one of the best (Table 1) after the MRTS series model with three zones.

[27] The MRTS models examined in this work are identical to the multirate mass transfer models used in groundwater hydrology [*Haggerty and Gorelick*, 1995]. The MRMT models were developed to address the limitations of single-rate, mobile-immobile models that show an exponential decay of solute concentration in the mobile phase by adding multiple rates of exchange between the two domains. This modification allowed descriptions of solute transport following nonexponential breakthrough. The connection between MRMT, fractional derivative and CTRW models is described by *Silva et al.* [2009]. The contribution of the present work lies in the observation that when transport is hydraulically controlled (e.g., when dispersion is the dominant mode of transport), the MRTS model should be modified to reflect the fact that the different exchange rates are triggered sequentially and not concurrently. An analogous situation in groundwater hydrology involves solute transport under the influence of external pumping. When the effects of imposed pumping dominate over natural

gradient flow and transport processes in aquifers, equations similar to the series MRTS model in this paper can be expected to apply. Recently *Phanikumar and McGuire* [2010] successfully used models similar to the series MRTS model to describe the transport of both conservative and nonconservative solutes in aquifers under the influence of external pumping (push-pull tests).

[28] Although it is tempting to relate the estimated parameters of the MRTS models to the physical characteristics of the river (e.g., sizes of storage zones, travel times, etc.), this can be a nontrivial task in a complex river system such as the St. Clair River; therefore this was not attempted. Similarly, a comparison of parameters from a multirate model with similar parameters of the standard TS model is generally confounded by the way the MRTS models disaggregate processes into different compartments as more storage zones are added. Finally, a few caveats of the approach used in this work are in order. To separate the contributions of surface storage (the focus of this study) from those of hyporheic storage, we have used calibrated 3-D flow and transport models to generate synthetic data in which there is no hyporheic exchange. Tracer data from natural rivers, however, will always include contributions from hyporheic storage; therefore, features such as bimodal or multimodal BTCs may or may not appear in real data depending on the extent to which the surface storage processes are modulated by hyporheic exchange. Our results based on the synthetic data, therefore, should be taken as being suggestive of the processes in large rivers rather than being conclusive. Further research on transport and storage zone dynamics in large rivers is clearly needed.

## 5. Conclusions

[29] Using synthetic data generated from calibrated, three-dimensional hydrodynamic and particle transport models, we tested several one-dimensional solute transport models for their ability to describe surface storage dynamics in a large international river. Multimodal breakthrough, a key aspect of the transport generated by river features such as islands and meander bends, could not be described using a single rate coefficient, an approach often used to describe surface storage in small rivers and streams. The standard TS model, the parallel MRTS models with different number of storage zones, and the fractional derivative (FSTS) model considered in this work all produced identical solutions at late time and failed to describe the multimodal nature of the BTCs. The series MRTS model, in which the different exchange rates are triggered sequentially, described the data better in addition to capturing the multimodal nature of the BTCs.

[30] **Acknowledgments.** This research was funded by the NOAA Center of Excellence for Great Lakes and Human Health. We thank J. Niu, Department of Civil and Environmental Engineering, Michigan State University for assistance with parameter estimation. Funding for the St. Clair River dye tracer release and 3-D hydrodynamic model development was provided by the Great Lakes Observing System (GLOS). The dye release, measurements, and initial processing were carried out by Applied Science Inc. (ASI), Detroit, MI.

## References

Anderson, E. J., and D. J. Schwab (2011), Relationships between wind-driven and hydraulic flow in Lake St. Clair and the St. Clair River Delta, *J. Great Lakes Res.*, 37, 147–158.

- Anderson, E. J., D. J. Schwab, and G. A. Lang (2010), Real-time hydraulic and hydrodynamic model of the St. Clair River, Lake St. Clair, Detroit River system, *J. Hydraul. Eng.*, 136(8), 507–518.
- Baeumer, B., M. M. Meerschaert, and E. Nane (2009), Space-time duality for fractional diffusion, *J. Appl. Prob.*, 46(4), 1100–1115.
- Basagaoglu, H., T. R. Ginn, C. T. Green, and B. J. McCoy (2002), Transport in heterogeneous media: Tracer dynamics in complex flow networks, *AIChE J.*, 48(5), 1121–1131.
- Bencala, K. E., and R. A. Walters (1983), Simulation of solute transport in a mountain pool-and-riffle stream—A transient storage model, *Water Resour. Res.*, 19(3), 718–724, doi:10.1029/WR019i003p00718.
- Benson, D. A. (1998), The fractional advection-dispersion equation: Development and application, Ph.D. thesis, University of Nevada, Reno.
- Berkowitz, B., J. Klafter, R. Metzler, and H. Scher (2002), Physical pictures of transport in heterogeneous media: Advection-dispersion, random-walk, and fractional derivative formulations, *Water Resour. Res.*, 38(10), 1191, doi:10.1029/2001WR001030.
- Berkowitz, B., A. Cortis, M. Dentz, and H. Scher (2006), Modeling non-Fickian transport in geological formations as a continuous time random walk, *Rev. Geophys.*, 44(2), RG2003, doi:10.1029/2005RG000178.
- Boano, F., A. I. Packman, A. Cortis, R. Revelli, and L. Ridolfi (2007), A continuous time random walk approach to the stream transport of solutes, *Water Resour. Res.*, 43(10), W10425, doi:10.1029/2007WR006062.
- Bradley, D. N., G. E. Tucker, and D. A. Benson (2010), Fractional dispersion in a sand bed river, *J. Geophys. Res.*, 115, F00A09, doi:10.1029/2009JF001268.
- Briggs, M. A., M. N. Gooseff, C. D. Arp, and M. A. Baker (2009), A method for estimating surface transient storage parameters for streams with concurrent hyporheic storage, *Water Resour. Res.*, 45, W00D27, doi:10.1029/2008WR006959.
- Briggs, M. A., M. N. Gooseff, B. J. Peterson, K. Morkeski, W. M. Wollheim, and C. S. Hopkinson (2010), Surface and hyporheic transient storage dynamics throughout a coastal stream network, *Water Resour. Res.*, 46, W06516, doi:10.1029/2009WR008222.
- Burnham, K. E., and D. R. Anderson (1998), *Model Selection and Inference: A Practical Information-Theoretic Approach*, Springer, Telos.
- Chakraborty, P., M. M. Meerschaert, and C. Y. Lim (2009), Parameter estimation for fractional transport: A particle-tracking approach, *Water Resour. Res.*, 45, W10415, doi:10.1029/2008WR007577.
- Chen, C., R. C. Beardsley, and G. Cowles (2006), An Unstructured Grid, Finite-Volume Coastal Ocean Model: FVCOM User Manual, Rep. SMASST/UMASSD-06-0602, 321 pp, Dartmouth, MA.
- Church, M. (1992), Channel morphology and topology, in *The Rivers Handbook*, edited by C. Calow and G. Petts, 2, 126–143, Blackwell, Oxford.
- D'Angelo, D. J., J. R. Webster, S. V. Gregory, and J. L. Meyer (1993), Transient storage in Appalachian and Cascade mountain streams as related to hydraulic characteristics, *J. North Am. Benthol. Soc.*, 12(3), 223–235.
- Deng, Z. Q., and H. S. Jung (2009), Variable residence time-based model for solute transport in streams, *Water Resour. Res.*, 45, W03415, doi:10.1029/2008WR007000.
- Deng, Z. Q., V. P. Singh, and L. Bengtsson (2004), Numerical solution of fractional advection-dispersion equation, *J. Hydraul. Eng.*, 130(5), 422–431.
- Deng, Z. Q., L. Bengtsson, and V. P. Singh (2006), Parameter estimation for fractional dispersion model for rivers, *Environ. Fluid Mech.*, 6(5), 451–475.
- Deng, Z. Q., H. S. Jung, and B. Ghimire (2010), Effect of channel size on solute residence time distributions in rivers, *Adv. Water Resour.*, 33(9), 1118–1127.
- De Smedt, F., W. Brevis, and P. Debels (2005), Analytical solution for solute transport resulting from instantaneous injection in streams with transient storage, *J. Hydrol.*, 315, 25–39.
- Fernald, A. G., D. H. Landers, and P. J. Wigington (2006), Water quality changes in hyporheic flow paths between a large gravel bed river and off-channel alcoves in Oregon, USA, *River Res. Appl.*, 22(10), 1111–1124.
- Ganti, V., M. M. Meerschaert, E. Foufoula-Georgiou, E. Viparelli, and G. Parker (2010), Normal and anomalous diffusion of gravel tracer particles in rivers, *J. Geophys. Res.*, 115, F00A12, doi:10.1029/2008JF001222.
- García, C. M., K. Oberg, and M. H. García (2007), ADCP Measurements of Gravity Currents in the Chicago River, Illinois, *J. Hydraul. Eng.*, 133(12), 1356–1366.
- Gillespie, J. L., and D. B. Dumouchelle (1989), Ground-water flow and quality near the upper Great Lakes connecting channels, Michigan, Rep., 89 pp, U.S. Geological Survey Water Resources Investigations Report 88-4232, Lansing, Michigan.
- Gooseff, M. N., J. LaNier, R. Haggerty, and K. Kokkeler (2005), Determining in-channel (dead zone) transient storage by comparing solute transport in a bedrock channel-alluvial channel sequence, Oregon, *Water Resour. Res.*, 41(6), W06014, doi:10.1029/2004WR003513.
- Gooseff, M. N., R. O. Hall, and J. L. Tank (2007), Relating transient storage to channel complexity in streams of varying land use in Jackson Hole, Wyoming, *Water Resour. Res.*, 43(1), W01417, doi:10.1029/2005WR004626.
- Haggerty, R., and S. M. Gorelick (1995), Multiple-rate mass-transfer for modeling diffusion and surface-reactions in media with pore-scale heterogeneity, *Water Resour. Res.*, 31(10), 2383–2400, doi:10.1029/95WR10583.
- Haggerty, R., S. A. McKenna, and L. C. Meigs (2000), On the late-time behavior of tracer test breakthrough curves, *Water Resour. Res.*, 36(12), 3467–3479, doi:10.1029/2000WR900214.
- Holtschlag, D. J., and J. A. Koschik (2002), A Two-Dimensional Hydrodynamic Model of the St. Clair–Detroit River Waterway in the Great Lakes Basin, Rep. 01-4236, 63 pp, USGS, Lansing, Michigan.
- Houser, J. N., D. W. Bierman, R. M. Burdis, and L. A. Soeken-Gittinger (2010), Longitudinal trends and discontinuities in nutrients, chlorophyll, and suspended solids in the Upper Mississippi River: Implications for transport, processing, and export by large rivers, *Hydrobiologia*, 651(1), 127–144.
- Kadlec, R. H. (1994), Detention and mixing in free-water wetlands, *Ecol. Eng.*, 3(4), 345–380.
- Marion, A., and M. Zaramella (2006), Effects of velocity gradients and secondary flow on the dispersion of solutes in a meandering channel, *J. Hydraul. Eng.*, 132(12), 1295–1302.
- Marion, A., M. Zaramella, and A. Bottacin-Busolin (2008), Solute transport in rivers with multiple storage zones: The STIR model, *Water Resour. Res.*, 44(10), W10406, doi:10.1029/2008WR007037.
- Neal, J., G. Schumann, P. Bates, W. Buytaert, P. Matgen, and F. Pappenberger (2009), A data assimilation approach to discharge estimation from space, *Hydrol. Processes*, 23(25), 3641–3649.
- Parsons, D. R., J. L. Best, S. N. Lane, O. Orfeo, R. J. Hardy, and R. Kostaschuk (2007), Form roughness and the absence of secondary flow in a large confluence-diffuence, Rio Parana, Argentina, *Earth Surf. Processes Landforms*, 32(1), 155–162.
- Phanikumar, M. S., and J. T. McGuire (2010), A multi-species reactive transport model to estimate biogeochemical rates based on single-well push-pull test data, *Comput. Geosci.*, 36(8), 997–1004.
- Phanikumar, M. S., I. Aslam, C. P. Shen, D. T. Long, and T. C. Voice (2007), Separating surface storage from hyporheic retention in natural streams using wavelet decomposition of acoustic Doppler current profiles, *Water Resour. Res.*, 43(5), W05406, doi:10.1029/2006WR005104.
- Pope, S. B. (2000), *Turbulent Flows*, pp 806, Cambridge University Press, New York.
- Runkel, R. L. (1998), One-dimensional transport with inflow and storage (OTIS): A solute transport model for streams and rivers, Rep. Water Resour. Invest. Rep. 98-4018, 73 pp, US Dept. of the Interior, US Geological Survey.
- Runkel, R. L., D. M. McKnight, and E. D. Andrews (1998), Analysis of transient storage subject to unsteady flow: diel flow variation in an Antarctic stream, *J. North Am. Benthol. Soc.*, 17(2), 143–154.
- Salehin, M., A. I. Packman, and A. Worman (2003), Comparison of transient storage in vegetated and unvegetated reaches of a small agricultural stream in Sweden: seasonal variation and anthropogenic manipulation, *Adv. Water Resour.*, 26(9), 951–964.
- Schmid, B. H. (2003), Temporal moments routing in streams and rivers with transient storage, *Adv. Water Resour.*, 26(9), 1021–1027.
- Schmid, B. H. (2004), Simplification in longitudinal transport modeling: case of instantaneous slug releases, *J. Hydrol. Eng.*, 9(4), 319–324.
- Schumer, R., D. A. Benson, M. M. Meerschaert, and B. Baeumer (2003), Fractal mobile/immobile solute transport, *Water Resour. Res.*, 39(10), 1296, doi:10.1029/2003WR002141.
- Shen, C., and M. S. Phanikumar (2009), An efficient space-fractional dispersion approximation for stream solute transport modeling, *Adv. Water Resour.*, 32(10), 1482–1494.
- Shen, C., M. S. Phanikumar, T. T. Fong, I. Aslam, S. P. McElmurry, S. L. Molloy, and J. B. Rose (2008), Evaluating bacteriophage P22 as a tracer in a complex surface water system: The Grand River, Michigan, *Environ. Sci. Technol.*, 42(7), 2426–2431.

- Shen, C., J. Niu, E. J. Anderson, and M. S. Phanikumar (2010), Estimating longitudinal dispersion in rivers using Acoustic Doppler Current Profilers, *Adv. Water Resour.*, 33(6), 615–623.
- Silva, O., J. Carrera, M. Dentz, S. Kumar, A. Alcolea, and M. Willmann (2009), A general real-time formulation for multi-rate mass transfer problems, *Hydrol. Earth Syst. Sci.* 13(8), 1399–1411.
- Smith, A. J., and C. P. Tran (2010), A weight-of-evidence approach to define nutrient criteria protective of aquatic life in large rivers, *J. North Am. Benthol. Soc.*, 29(3), 875–891.
- Smith, L. C., and T. M. Pavelsky (2008), Estimation of river discharge, propagation speed, and hydraulic geometry from space: Lena River, Siberia, *Water Resour. Res.*, 44(3), W03427, doi:10.1029/2007WR006133.
- Tank, J. L., E. J. Rosi-Marshall, M. A. Baker, and R. O. Hall (2008), Are rivers just big streams? A pulse method to quantify nitrogen demand in a large river, *Ecology*, 89(10), 2935–2945.
- Wheatcraft, S. W., and M. M. Meerschaert (2008), Fractional conservation of mass, *Adv. Water Resour.*, 31(10), 1377–1381.
- Worman, A. (2000), Comparison of models for transient storage of solutes in small streams, *Water Resour. Res.*, 36(2), 455–468, doi:10.1029/1999WR900281.
- Zhang, Y., D. A. Benson, and D. M. Reeves (2009), Time and space nonlocalities underlying fractional-derivative models: Distinction and literature review of field applications, *Adv. Water Resour.*, 32, 561–581.

---

E. J. Anderson, Cooperative Institute for Limnology and Ecosystems Research, University of Michigan, Ann Arbor, MI, USA. (ejander@umich.edu)

M. S. Phanikumar, Department of Civil and Environmental Engineering, Michigan State University, East Lansing, MI, USA. (phani@msu.edu)